Rare Met. (2019) 38(6):577–587
https://doi.org/10.1007/s12598-019-01273-8

RARE METALS
www.editorialmanager.com/rmet

Mg-based absorbable membrane for guided bone regeneration (GBR): a pilot study

Wei Peng, Jun-Xiu Chen, Xian-Feng Shan, Yi-Chuan Wang, Fan He, Xue-Jin Wang*, Li-Li Tan*, Ke Yang

Received: 30 November 2018 / Revised: 28 December 2018 / Accepted: 18 February 2019 / Published online: 11 May 2019

Abstract A novel calcium-phosphate (Ca–P)-coated magnesium (Mg) membrane used for guided bone regeneration (GBR) was studied. The microstructural characterization, electrochemical test, immersion test, fluorescence labeling analysis and histopathological evaluation were carried out. The results showed that Ca–P coating could obviously improve the corrosion resistance of the pure Mg membrane. The in vivo results showed that Mg membrane coated with Ca–P would take 8 weeks to be completely absorbed. However, Mg membrane was completely absorbed within 1 week. Histopathological evaluation showed that the Ca–P-coated Mg membranes were significantly better than Ti membranes at the early implantation time (4 weeks), and with the time prolonging, the performance of the coated Mg membrane was not as good as pure Ti membranes (but still better than blank group) at 8 and 12 weeks. The coated biodegradable Mg membrane had a good promising application in GBR. But further studies have to be done to further decrease the degradation rate of pure Mg membrane.

Keywords Bone defect; Guided bone regeneration; Ca–P-coated magnesium (Mg) membrane; Bioabsorbable membrane

1 Introduction

Nowadays, dental implants have been widely used for the treatment of dental defect. At the implant interface, bone quality and its quantity play important roles in determining stability of the implant system. Bone insufficiency, resulting from alveolar bone resorption after dental extraction and bone defects infected by periodontal diseases, remains a major challenge for the insertion of dental implants.

Guided bone regeneration (GBR) has been introduced and combined with bone augmentation to restore the bone adjacent to dental implants [1]. The principle of GBR is the separation of bone graft material from the surrounding fibrous tissue, which allows for bone regeneration [2]. Thus, the key point of this established procedure is the success of bone graft material contained inside the defect region, which is covered by a separating barrier membrane to stabilize graft material and prevents periodontal infection and ingrowth of surrounding fibrous tissue. The concept has been applied in periodontal regeneration and alveolar augmentation therapy [3, 4], and high success rates of GBR procedures of more than 95% have been reported in recent years [5, 6].

Conventional GBR barrier membranes can be classified into two material systems, namely non-degradable membranes and degradable membranes [7]. Non-degradable

Wei Peng and Jun-Xiu Chen have contributed equally to this work and should be regarded as co-first authors.

W. Peng, X.-J. Wang*
Department of Stomatology, Affiliated Zhongshan Hospital of Dalian University, Dalian 116001, China
e-mail: wxj0411@aliyun.com

W. Peng, X.-F. Shan, Y.-C. Wang, F. He
Medical School of Dalian University, Dalian 116622, China

J.-X. Chen, L.-L. Tan*, K. Yang
Institute of Metal Research, Chinese Academy of Sciences, Shenyang 110016, China
e-mail: lltan@imr.ac.cn

J.-X. Chen
School of Materials Science and Engineering, University of Science and Technology of China, Shenyang 110016, China

membranes, such as polytetrafluoroethylene and titanium (Ti), could provide high volume stability and have achieved excellent results in clinic [8, 9]. However, after the new bone regeneration, a second surgery is required for membrane removal before the insertion of dental implants, which means that it could significantly increase the risks of infection, pain and healing period [10]. Also, the material's rigidity may lead to wound dehiscence during healing, and poor adaptability, which could cause clinical problems such as infection and ingrowth of surrounding fibrous tissue [11].

Owing to the limitations of non-degradable membranes, the application of degradable membranes in clinic has attracted increasing interest. Collagen membranes are most commonly used and have shown favorable biocompatibility and bioresorbability [12]. With the advantage of being resorbed by the body, a second surgery for degradable membrane removal is not required. This reduces the risk of infection, tissue damage and onset of pain. However, collagen membranes have variable degradation rates and do not offer appropriate volume stability due to their low mechanical strength and stiffness [13]. If the membrane resorbs too rapidly, there will be no sufficient support for the defect region. This could be a clinical problem especially in large bone defect reconstruction that the space for bone growth will reduce when the defect region is exposed to the surrounding fibrous tissue.

In response to these clinical problems, this pilot study aims to develop a new type of barrier membrane that can feature adequate mechanical stability and biodegradability in achieving more consistent and effective bone regeneration. Magnesium (Mg) is attracting immense attention as a promising biodegradable material and differs from other biomaterials due to its unique performance in biocompatibility and biomechanical properties [14, 15]. Moreover, as one of the required metals for the metabolism, Mg is present in body and can accelerate cell proliferation and wound healing [16]. Therefore, magnesium-based materials show great potential as barrier membranes for dental GBR procedures. However, poor corrosion resistance in physiological environments limits its clinical applications. Rapid solidification technology could refine the grain size of Mg alloys, extend solid solubility and make the composition homogeneous [17], which is beneficial to the corrosion resistance of Mg alloys, and thin membrane can be achieved more easily by rapid solidification technique compared with commonly used rolling and extrusion techniques. So, in this work, rapid solidification was adopted to fabricate pure Mg membrane. In addition, some recent studies and our previous works have confirmed that surface treatment can significantly improve the corrosion resistance of magnesium-based implants [18]. Calcium phosphate (Ca–P) coating is non-toxic and can improve the biocompatibility of implants [19]. In this pilot study, we investigated the feasibility of using Ca–P-coated Mg membrane for guided bone regeneration (GBR).

2 Experimental

2.1 Fabrication of pure Mg membranes

A mixture of pure Mg (> 99.95%) was melted in a quartz tube under an argon atmosphere in an induction furnace, and then, the pure Mg was injected into the copper rolling which is rolling at the speed of 1500 $m \cdot min^{-1}$. Pure Mg membrane with the thickness of 50 μm was fabricated. The pure Mg membrane was cut into square shape with the width of 8 mm.

2.2 Fabrication of Ca–P coating

The pure Mg membrane was immersed in 0.1 $mol \cdot L^{-1}$ KF solution for 24 h first, and subsequently, the samples were immersed in a mixed solution of $NaNO_3$, $Ca(H_2PO_4)_2 \cdot H_2O$ and H_2O_2 for 24 h. A constant temperature of 20 °C was maintained. After immersion, the samples were cleaned with absolute ethanol and dried in air. Pure Ti screw (1802-15-05, Xi'an Zhongbang Titanium Biological Materials Co., Ltd., Xi'an, China) was used to fix the pure Mg membrane. Diameter of head, tip diameter and length are 2.50, 0.45 and 1.23 mm, respectively. Micro-arc oxidation (MAO) coating was fabricated on the pure Ti screw in order to avoid the galvanic corrosion between the pure Ti and pure Mg membrane. The detailed method was the same with our previous work [20].

2.3 In vitro tests

The microstructure of the coated Mg membrane was observed by a scanning electron microscope (SEM, S-3400N). Energy-dispersive spectrum (EDS) was used to analyze the composition of the coating. The coated Mg membrane with a surface area of 0.64 cm^2 was used for the electrochemical test. The test was performed by using Gamry Instruments (Reference 600). A three-electrode system was used for the test, and the detailed parameters were the same with our previous work [21]. The test was repeated three times for each coating. The coated Mg membranes were immersed in a Hank's solution for 2 weeks. The immersion ratio was 1.25 $cm^2 \cdot ml^{-1}$. The Hank's solution was changed every day in order to keep the solution fresh. The pH value was measured for 2 weeks. After immersion, the samples were cleaned in chromium trioxide solution. The corrosion rate was calculated [22].

Then, the morphology of the coated Mg membrane was observed by SEM.

2.4 In vivo tests

2.4.1 Animals and ethics

Nine healthy male New Zealand White rabbits, aged 6 months and weighing 2.5–3.0 kg, were used in this study. The Ethics Committee for Clinical Trials of Affiliated Zhongshan Hospital of Dalian University approved the study protocol (No. DW2018-054). The experimental animals were provided by Animal Testing and Research Center of Dalian Medical University (Dalian, China) and cared in accordance with international standards on animal welfare by the Animal Research Committee of the hospital. Each rabbit was kept in a single cage under observation and supervision for 1 week before the experiment to monitor the behavior. Standard quantity and quality of diet and water drinking were permitted.

2.4.2 Surgical procedure

The surgical procedure was performed under strict sterile conditions. General anesthesia was induced during all surgical procedures. After the intravenous injection of pelltobarbitalum natricum 30 $mg \cdot kg^{-1}$ and intramuscular injection of xylazine hydrochloride 0.1 $mg \cdot kg^{-1}$ with standard monitoring, local anesthesia was performed with Primacaine. Then, chlorhexidine gluconate solution (0.05%) was used to cleanse the skull region. The soft tissue and periosteum were carefully raised following a midline incision. There were a total of four circular osseous defects with 6.0 mm in diameter and 1.3 mm in depth made with a surgical bur, and no damage to dura was ensured. The distance between the edges of adjacent defects was at least 4 mm. The periosteum over each osseous defect was completely removed to avoid the contribution to the GBR procedures in the study. The bone harvested from the defect region was prepared to fill the defects as autologous bone powder. The defects of each rabbit were assigned to receive Ca–P-coated Mg membrane, pure Ti membrane, pure Mg membrane and no membrane (Fig. 1). Then, all membranes were applied over the autologous bone powder and fixed with micro-screws. And the distance between the edges of the adjacent membranes is at least 2 mm. The wound was closed and close postoperative observation was taken. Figure 2 shows the surgical procedure. Surgical inspection under local anesthesia on randomly selected four rabbits at 1 week and 2 weeks after surgery was taken to evaluate the absorption of membranes, and two of the four were used at each time point. And subcutaneous puncture procedure to all rabbits

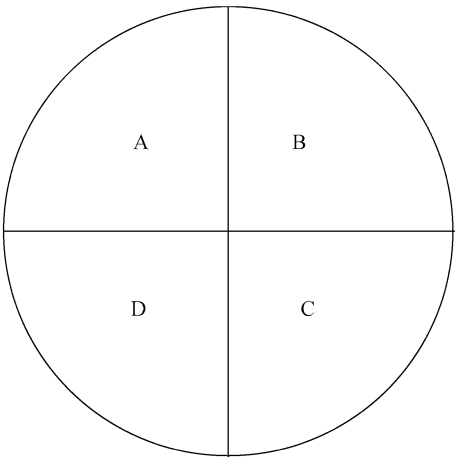

Fig. 1 Assignment of different membranes over defect regions A Ca–P-coated Mg membrane, B pure Mg membrane, C blank and D pure Ti membrane

at 1 week after surgery was performed to leak the hydrogen cavity. No more damage to the defect region was ensured.

2.4.3 Samples harvest

Three of nine rabbits were randomly selected and killed at 4, 8 and 12 weeks post-surgery, respectively. And the fluorescence labeling was performed with calcein fluorescent dye (Sigma, USA) by intramuscular injection before killing them. An incision was made over the old incision, and tissues were carefully dissected. The tissue/bone blocks containing reconstructed bone and its surrounding native bone were harvested and immediately placed into 70% ethanol for fixation.

2.4.4 Micro-CT

Micro-CT images of all bone/tissue blocks were photographed on a micro-CT system (80 V, 500 μA; Siemens, Germany) with a resolution of 9.47 μm. And the three-dimensional (3D) images were reconstructed and measured by Mimics 17.0 software. Then, the measurements of bone volume density (BV/TV) around the defect region were given by these 3D images.

2.4.5 Fluorescence labeling observation and histomorphometric evaluation

After fixation and embedding, all bone/tissue blocks were made into hard tissues sections. First, the bone/tissue blocks were dehydrated in graded series of ethanol (70% up to 100%). Then, all were thoroughly rinsed in tap water and infiltrated in pure resin. After that, the specimens were embedded in pure resin. Finally, by using the Exakt sawing

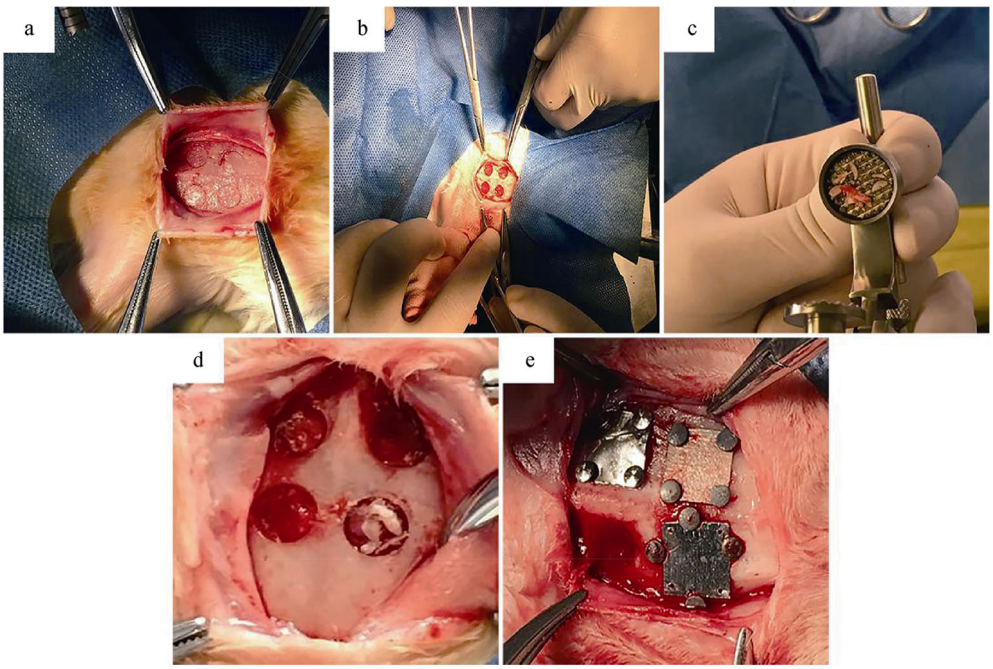

Fig. 2 Surgical procedures: **a** raising soft tissue and periosteum, **b** surgically creating bone defects with preservation of underlying dura, **c** grinding bone harvested from surgery into autologous bone powder, **d** placement of autologous bone powder into defect site and **e** placement and fixation of membranes over defect region

and grinding equipment (Exakt Apparatebau, Norderstedt, Germany), the sections obtained were cut into size of about 50–60 μm. All sections were observed by a confocal laser scanning microscopy (LSM, Nikon, Japan). Then, the sections were stained with hematoxylin–eosin (H&E) to visualize the evidence of new bone formation and examined using a light microscope (XD-202, Nanjing Jiangnan Novel Optics Co., Ltd., Nanjing, China).

2.4.6 Statistical analysis

After one-way analysis of variance (ANOVA) test was performed to analyze the parametric data (reported as mean ± standard deviation), post hoc comparisons of means were carried out with the Student–Newman–Keuls (S–N–K) analysis. A value of $P < 0.05$ was considered statistically significant.

3 Results

3.1 Microstructural characterization

Figure 3 presents the microstructure and EDS analysis of the coated pure Mg membrane. It can be observed that the grain size of the pure Mg membrane was about 2–5 μm (Fig. 3a). There were many randomly distributed lamellar depositions on the surface of the coated Mg membrane (Fig. 3b). The thickness of the Ca–P coating was not uniform. The thickness ranged from 10 to 70 μm (Fig. 3c). According to EDS analysis, it can be inferred that the composition of the coating was mainly calcium phosphate (Fig. 3d).

3.2 In vitro experiments

3.2.1 Electrochemical tests

Figure 4 and Table 1 present the potentiodynamic polarization curves and the Tafel fitting results. It can be seen that the corrosion current density (i_{corr}, $\mu A \cdot cm^{-2}$) of Ca–P-coated Mg (4.78 $\mu A \cdot cm^{-2}$) was much lower than that of uncoated pure Mg (8.50 $\mu A \cdot cm^{-2}$) and the corrosion rate (P_i, $mm \cdot year^{-1}$) was calculated according to the following equation [22]:

$$P_i = 22.85 i_{corr} \quad (1)$$

The corrosion rate of uncoated pure Mg (0.19 $mm \cdot year^{-1}$) was about two times higher than that of Ca–P-coated Mg membrane (0.11 $mm \cdot year^{-1}$). Figure 5 shows the impedance curves of the coated Mg membrane. Figure 5a shows the relationship between the real part and imaginary part. Figure 5b shows the relationship between the impedance modulus and phase angle with the frequency. From the Nyquist curves, it can be seen that there are a large capacitive loop and a small inductive loop.

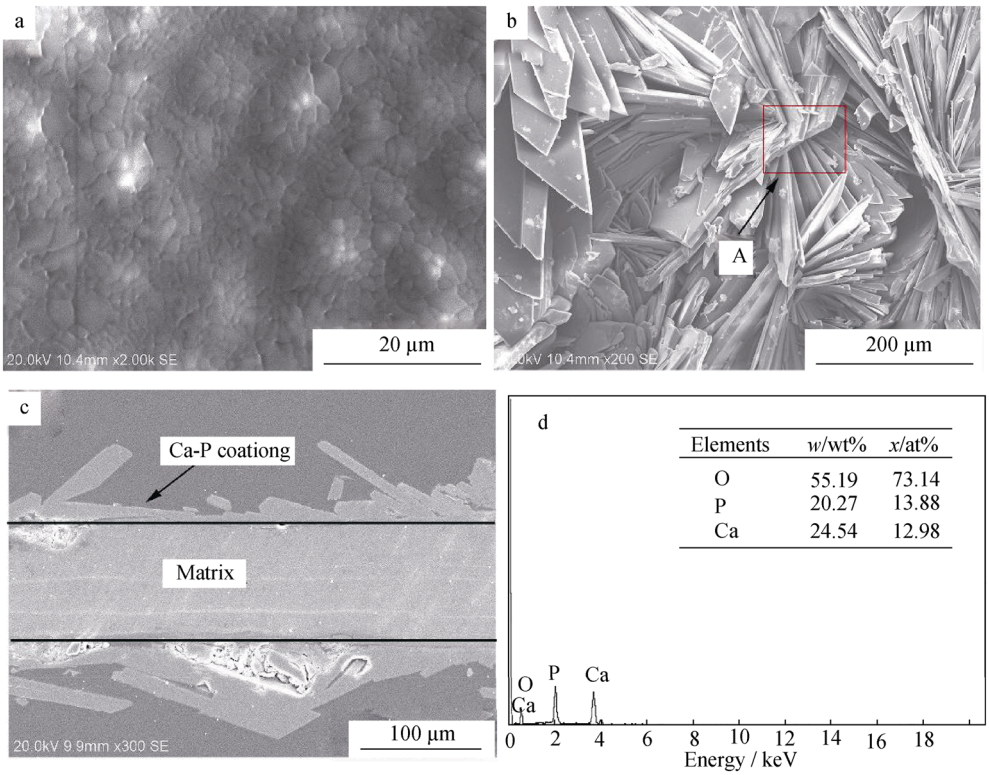

Fig. 3 SEM images of **a** pure Mg membrane, **b** surface and **c** cross section of coated Mg membrane; **d** EDS analysis of Area A marked in **b**

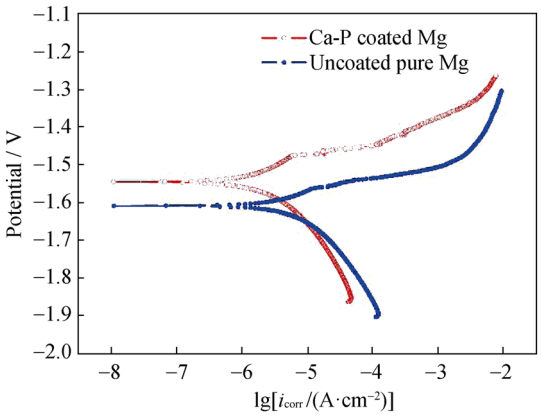

Fig. 4 Potentiodynamic polarization curves of three coatings in Hank's solution

Table 1 Tafel fitting results based on potentiodynamic polarizations tested in Hank's solution

Materials	i_{corr}/(μA·cm^{-2})	E_{corr}/V	P_i/(mm·year^{-1})
Ca–P coated Mg	4.78 ± 1.28	− 1.56 ± 0.03	0.11 ± 0.03
Uncoated pure Mg	8.50 ± 0.94	− 1.60 ± 0.01	0.19 ± 0.02

Usually, the larger diameter of the capacitive loop means the better corrosion resistance. In addition, the value of Bode curve at low frequency is also closely related to the corrosion resistance. The higher the value is, the better the corrosion resistance is. Therefore, it can be concluded that the corrosion resistance of Ca–P-coated Mg was much better than that of uncoated pure Mg. The electrochemical impedance spectroscopy (EIS) curves are fitted by Gamry Echem Analyst software with the errors less than 5%. The equivalent circuit [22] is presented in Fig. 5a. There were also double layers for the uncoated pure Mg. The corrosion products on the pure Mg membrane surface could act as a protective layer. Therefore, the equivalent circuit was the same for the coated and uncoated pure Mg membranes. Both R_1 (film resistance) and R_2 (charge transfer resistance) were closely related to the corrosion resistance. R_1 value of coated Mg was larger than that of uncoated pure Mg, indicating that the coating had a good protective effect. In addition, R_2 value of coated Mg was also larger than that of uncoated pure Mg, indicating that the charge transfer resistance of the coated Mg was higher than that of uncoated pure Mg. L represents the inductance between the hydrogen and the substrate. R_s is the Hank's solution resistance. CPE_1 is the capacity between the corrosion products layer and the solution. CPE_2 is the capacity between the matrix and the solution.

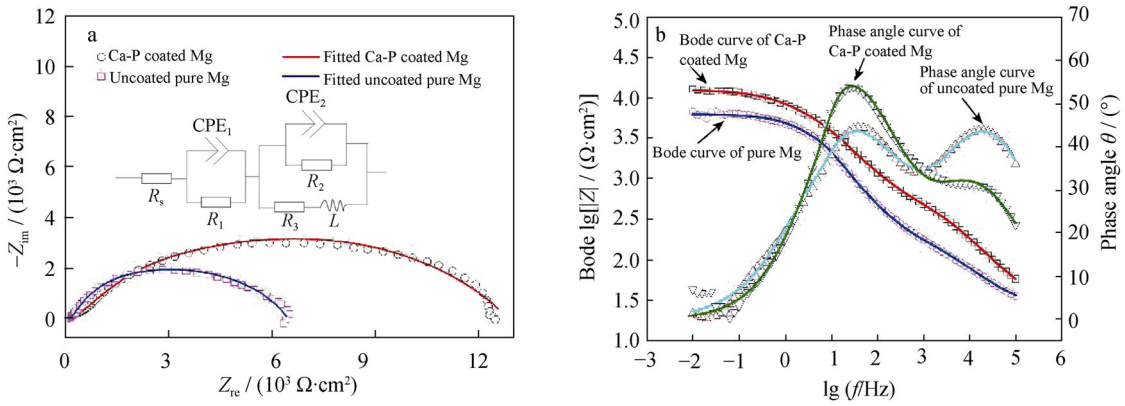

Fig. 5 Impedance curves: **a** Nyquist curves and **b** Bode and phase angle curves

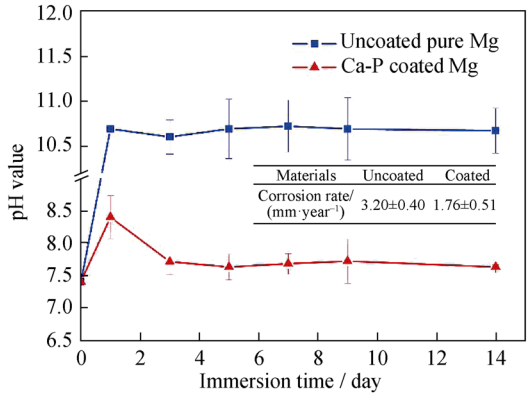

Fig. 6 pH change in pure Mg membrane at different immersion time in Hank's solution

3.2.2 *Immersion test*

Figure 6 shows the pH change in the coated and uncoated pure membrane in Hank's solution. It can be observed that the pH value of the uncoated pure Mg was much higher than that of the coated Mg. After 3-day immersion, the pH value of the Ca–P-coated Mg was stabilized at about 7.8. However, the pH value of the uncoated pure Mg was stabilized at about 10.7. In addition, the corrosion rate is also shown in Fig. 6. The corrosion rate of uncoated pure Mg was about 3.20 mm·year^{-1} which was much higher than that of Ca–P-coated Mg membrane (1.76 mm·year^{-1}). Figure 7 shows the corrosion morphologies of the coated and uncoated pure Mg membrane. It can be seen that the coated Mg exhibited good corrosion resistance without severe corrosion pits observed. However, the uncoated pure Mg was severely corroded with obvious pitting corrosion observed (Fig. 7).

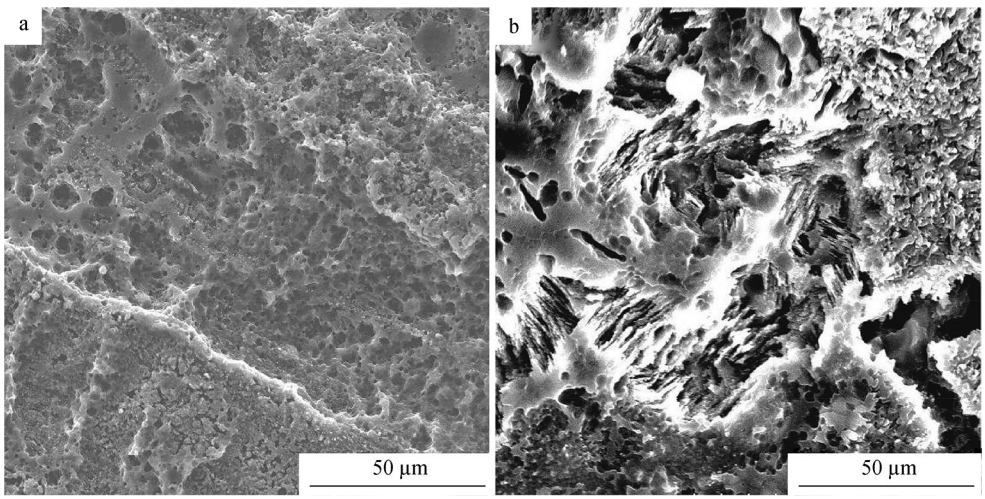

Fig. 7 Corrosion SEM images of pure Mg membrane with removal of corrosion products after 14-day immersion: **a** Ca–P-coated Mg and **b** uncoated pure Mg

Table 2 Fitting results of materials immersed in a Hank's solution

Specimens	$R_s/(\Omega\cdot cm^2)$	CPE_1		$R_1/(\Omega\cdot cm^2)$	CPE_2		$R_2/(\Omega\cdot cm^2)$	$R_3/(\Omega\cdot cm^2)$	$L/(H\cdot cm^{-2})$
		$Y_{01}/(S\cdot s^n\cdot cm^2)$	n_1		$Y_{02}/(S\cdot s^n\cdot cm^2)$	n_2			
Ca–P coated Mg	23.99	3.48×10^{-6}	0.70	0.33×10^3	18.49×10^{-6}	0.60	21.92×10^3	29.04×10^3	403.30
Uncoated pure Mg	22.96	18.80×10^{-6}	0.60	0.13×10^3	23.25×10^{-6}	0.70	18.78×10^3	9.43×10^3	148.70

Table 3 Measurements and analysis results of BV/TV at different time points (mean ± standard deviation, %)

Week	Type of membranes				*F* value	*P* value
	Blank	Pure Ti membrane	Pure Mg membrane	Coated Mg membrane		
4	33.687 ± 0.035◆	35.954 ± 0.042●	26.701 ± 0.013◆	38.785 ± 0.049	21.751	0.000334
8	35.094 ± 0.017◆	43.723 ± 0.033●	29.864 ± 0.019◆	40.519 ± 0.021	20.448	0.000415
12	42.976 ± 0.019●	55.963 ± 0.053◆	37.689 ± 0.048◆	48.537 ± 0.088	14.127	0.001462

◆$P < 0.05$ Ca–P-coated Mg membrane group versus blank, pure Ti membrane as well as pure Mg membrane group; ●$P > 0.05$ Ca–P-coated Mg membrane group versus blank, pure Ti membrane as well as pure Mg membrane group

3.3 In vivo experiments

In general, all rabbits remained stable after the bone defect protocol surgery. During surgical inspection and killing, no significant signs of infection or wound dehiscence were identified in all defect regions. From the surgical inspection and observation before killing, small subcutaneous gas pockets over membranes of all rabbits were noted at 1 week; after the leak of hydrogen, no significant signs of subcutaneous gas pockets were noted; at 1 week after surgery, the Mg membranes were visually no longer left; at 1 and 2 weeks, there were no significant visual area changes in Ca–P-coated Mg membranes; at 4 weeks, there were two-thirds of area of Ca–P-coated Mg membranes visually left; and at 8 weeks, there were no Ca–P-coated Mg membranes existed (Table 2).

3.3.1 Micro-CT

The measurements and analysis results are summarized in Table 3, including *F* value and *P* value (between groups ANOVA). During the observation period, all groups exhibited an increase in BV/TV. At Week 4, Ca–P-coated Mg membrane performed the highest BV/TV; however, there was no significant difference between Ca–P-coated Mg membrane group and pure Ti membrane group. Pure Mg membrane group was the lowest group. At Week 8 and Week 12, BV/TV measurements of pure Ti membrane group were both significantly higher than those of Ca–P-coated Mg membrane group. There was a significant difference between pure Mg membrane group and blank group at Week 8; in contrast, there was no significant difference found between the two groups at Week 12. Compared with the pure Mg membrane group and blank group, the 3D image of bone defect under Ca–P-coated Mg membrane at Week 12 obviously showed the formation of mature bone (Fig. 8).

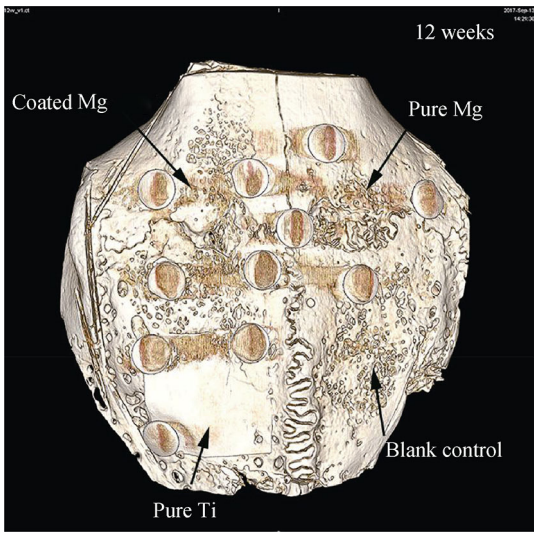

Fig. 8 3D image of bone defects at Week 12

3.3.2 Fluorescence labeling observation

At the end of 4, 8 and 12 weeks, the fluorescence labeling observation was taken to evaluate the bone mineralization (Fig. 9). With the increase in time, the fluorescent intensity of all groups increased; the pure Mg membrane group was the worst performance group compared with blank group at Week 12. At Week 4, the fluorescent intensity of Ca–P-

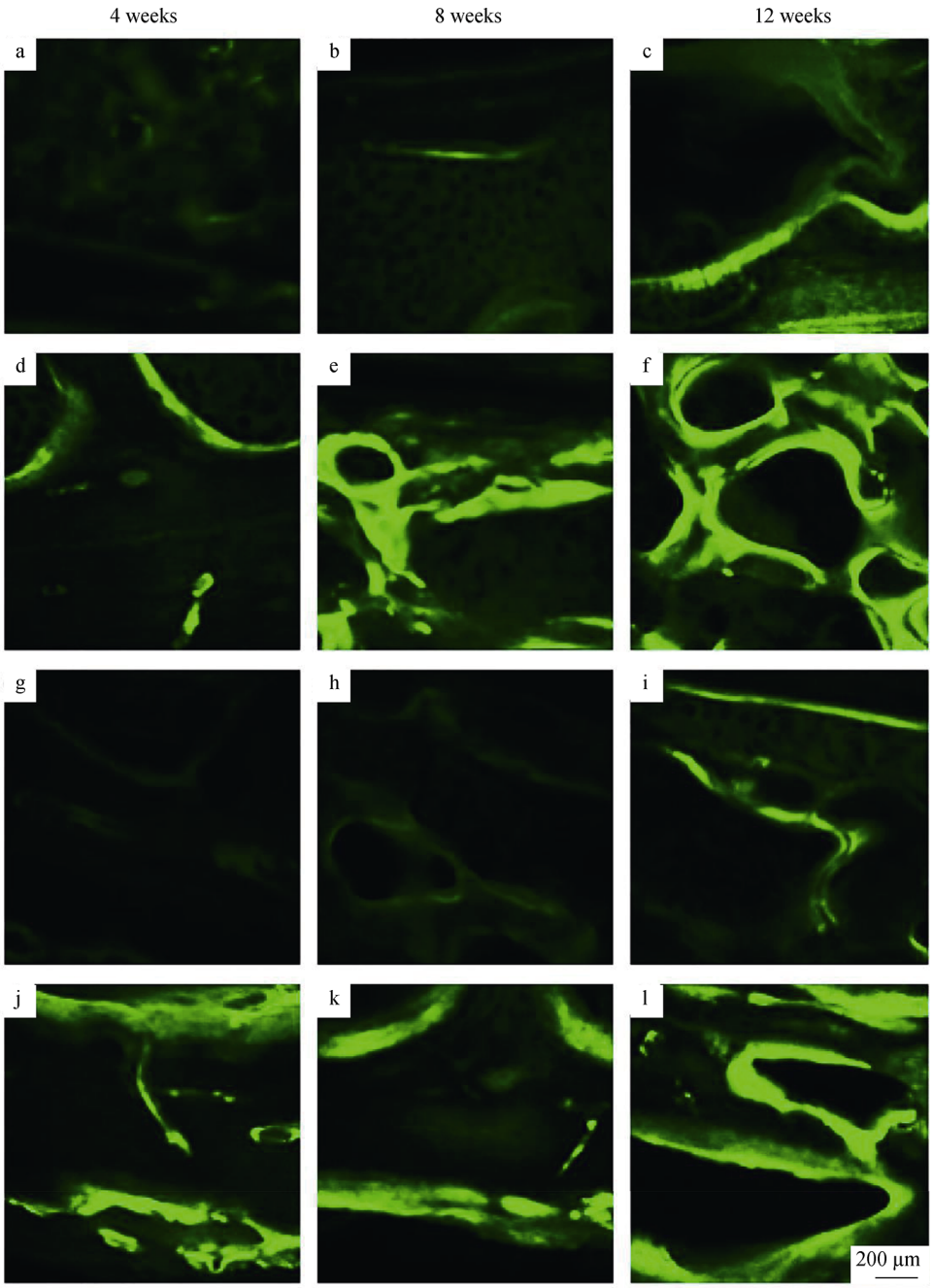

Fig. 9 Fluorescence images of **a–c** blank group, **d–f** pure Ti membrane group, **g–i** pure Mg membrane group and **j–l** Ca–P-coated Mg membrane group at 4, 8 and 12 weeks, respectively

coated Mg membrane group was slightly higher than that of pure Ti membrane group and significantly higher than that of blank group. At Week 8, the fluorescent intensity of Ca–P-coated Mg membrane group was slightly lower than that of Ti membrane group and significantly higher than that of blank group. At Week 12, the pure Ti membrane group was the highest group, and the fluorescent intensity of Ca–P-coated Mg membrane group was still significantly higher than of blank group.

3.3.3 Descriptive histology

The histological sections showed that all groups had new bone formed around the bone graft (Fig. 10). There were traces of mature bone formation at 4 weeks and more mature bone formation at 8 and 12 weeks. And no soft tissue infiltration was noted during the observation period. At Week 4, the Mg membranes over the bone defect regions were no longer present. In comparison, the Ca–P-

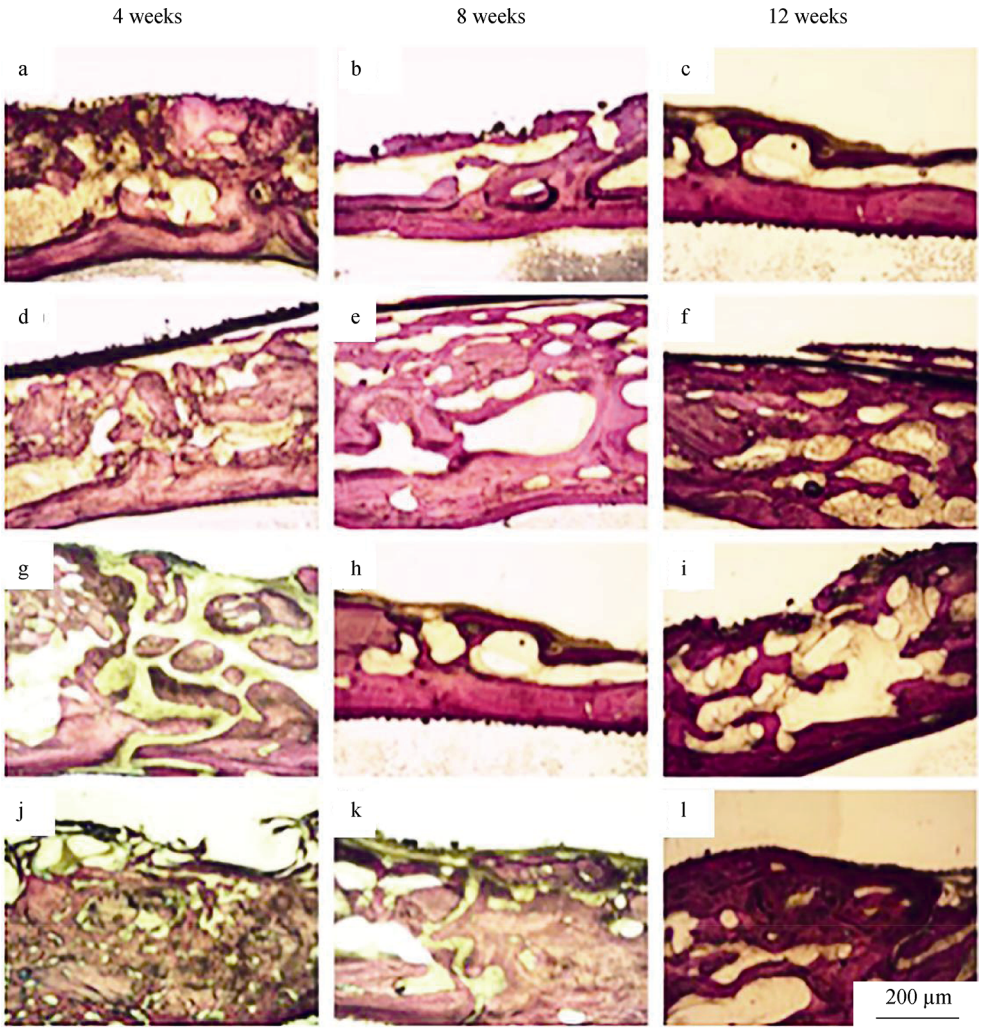

Fig. 10 H&E observation of **a–c** blank group, **d–f** pure Ti membrane group, **g–i** pure Mg membrane group and **j–l** Ca–P-coated Mg membrane group at 4, 8 and 12 weeks, respectively

coated Mg membranes were mostly present at the point of harvest. The new bone formation of the Ca–P-coated Mg membrane group was relatively better than that of pure Ti membrane group and significantly better than that of blank group. However, the Ca–P-coated Mg membranes in volume at Week 8 were less than that at Week 4 and were no longer present at Week 12. At Week 8 and Week 12, the new bone formation of the Ca–P-coated Mg membrane group was worse than that of pure Ti membrane group and still significantly better than that of blank group. In the absence of a barrier membrane, the new bone formation of pure Mg membrane group was the worst at Week 4 and Week 8 and comparable to that of the blank group at Week 12.

4 Discussion

In this pilot study, the investigation of Ca–P-coated Mg membranes in GBR procedures was performed by comparing three different barrier membranes in a rabbit model. Mg materials were promising candidates for new types of membranes for GBR due to its favorable biodegradation, mechanical stability and biocompatibility. However, the poor corrosion resistance of Mg has been a major obstacle to its clinical applicability. Results from previous works showed that the Ca–P coating significantly promoted the surface bioactivity of Mg implants and enhanced the corrosion resistance [23, 24]. By the use of Ca–P coating, we have evaluated the performance of biodegradable Mg for barrier membranes. As a result, the Ca–P coating was deposited on Mg membranes and the surface structure observed by SEM shows that the coating was compact but non-uniform. Energy-dispersive spectroscopy (EDS) analysis indicates that the coating is mainly composed of Ca, P and O. From the electrochemical experimental result, it can be seen that the corrosion rate of uncoated pure Mg was four times higher than that of Ca–P-coated Mg membrane. Moreover, the coated Mg

membrane exhibited more uniform corrosion than the uncoated pure Mg membrane.

The ultimate goal was to develop a novel barrier membrane with a reasonable degradation rate and adequate mechanical stability to be used as a volume-stable membrane in GBR with no requirement for removal. The mechanical properties of the pure Mg membrane provide the sufficient volume stability. The performance in physiological environments counts heavily in the development. Currently used volume-stable barrier membranes are made of Ti or reinforced by Ti, achieving excellent results in clinic. Thus, we compared the pure Ti membranes with the Ca–P-coated Mg membranes in a clinically relevant rabbit model. The pure Mg membrane group and blank group (absence of a membrane) were set to verify the in vivo enhancement of corrosion resistance and bioactivity. Micro-screws were used for fixation to avoid the movement and dehiscence. The study showed spontaneous bone healing in rabbit calvarial defects, which is in agreement with Delgado-Ruiz et al. [25]. However, the superior bone healing was noted where the Ti membranes or the Ca–P-coated Mg membranes covered. Owing to high corrosion rate, pure Mg membranes were no longer left and small subcutaneous gas pockets cover membranes due to that the formation of hydrogen was also noted when the first surgical inspection was performed at 1 week post-surgery. The performance of pure Mg membrane group at Week 4 in terms of BV/TV measurement and histology observation indicated that hydrogen bubbles may have negative effects on bone regeneration and delay the healing of surgical region. This is in agreement with the report by Song et al. [26]. After inspection, with the release of hydrogen bubbles, the performance of pure Mg membrane group with the absence of membrane was comparable to that of blank group at Week 12. In comparison, the significant absorption of Ca–P-coated Mg membranes was not visually noted during the surgical inspection at 1 and 2 weeks post-surgery and visually identified at 4 weeks post-surgery. No significant signs of subcutaneous gas pockets were visually and tactilely noted after the first surgical inspection. This indicated that the hydrogen resulting in that subcutaneous gas pockets was mainly from the absorption of Mg membrane. All Ca–P-coated Mg membranes were no longer left at Week 8. In agreement with the in vitro results, this result suggested that the Ca–P coating significantly promotes the corrosion resistance in vivo. Interestingly, by comparing the observation at Week 2 (hydrogen had been leaked and Ca–P-coated Mg membranes were not significantly absorbed) with Week 8 (the Ca–P-coated Mg membranes were totally absorbed), it appeared that the hydrogen from the absorption of Ca–P-coated Mg membranes was low. This suggested that the thin thickness of membrane, low amount of Mg and low corrosion rate of Ca–P-coated Mg membrane contribute to lower amount and slower production of hydrogen. Moreover, the hydrogen may be slowly adsorbed by the rabbit during the observation period. At Week 4, the Ca–P-coated Mg membrane group exhibited significantly better bone regeneration due to the bioactivity of Ca–P coating. With the resorption of membranes and formation of hydrogen bubbles, the pure Ti membrane group was increasingly better than the Ca–P-coated Mg membrane group at Week 8 and Week 12. The BV/TV measurement, fluorescence labeling observation and histology observation confirmed this. This suggested that the Ca–P-coated Mg membranes may achieve relatively better results than Ti membranes in clinic with the duration of membrane. Not only the Ca–P coating but also the Mg ions acts effective roles in bone regeneration during the absorption of Ca–P-coated Mg membranes. In a recent study, with subcutaneous puncture procedure to leak the hydrogen cavity, Lin et al. [27] concluded that a higher degradation amount of Mg would contribute to superior bone regeneration ability. They also discovered excellent outcomes in dentistry application of Mg-based materials. This property, compared to other biomaterials such as collagen and Mg alloys, will significantly reduce the potential risk of alloying elements or inflammatory reaction due to the introduction of desirable biocompatibility and low antigenicity biomaterial, which is named as the foreign body reaction [28, 29]. This might have significantly positive effects on the reconstruction of large bone defects [30].

Ca–P-coated Mg membrane exhibited better bioactivity than pure Ti membrane at the early implantation time (before 4 weeks). With implantation time prolonging, the coated Mg membrane could not meet the clinical service time (at least 12 weeks), which is due to its low thickness (50 μm) and fast degradation. Therefore, increasing the thickness of the pure Mg membrane and in further controlling the degradation rate of the membrane will be tried in the future study. However, from this preliminary investigation, it has been shown that Ca–P-coated Mg membrane has a good promising application for GBR.

5 Conclusion

This pilot study investigated the clinical effectiveness of a Ca–P-coated Mg membrane and provided directions for further study of Mg membrane for GBR. The Ca–P coating significantly promotes the corrosion resistance of Mg membrane both in vitro and in vivo. The Ca–P-coated Mg membranes may achieve relatively better results than pure Ti membranes in clinics with the duration of membrane, in terms of the BV/TV at Week 4. The duration time still

cannot meet the clinical demand, and related experiments to improve the quality of the coating are undergoing.

Acknowledgements This work was financially supported by the Key Program of China on Biomedical Materials Research and Tissue and Organ Replacement (Nos. 2016YFC1101804 and 2016YFC1100604) and Shenyang Key R&D and Technology Transfer Program (No. Z18-0-027).

References

[1] Cho KS, Choi SH, Han KH, Chai JK, Wikesjo UME, Kim CK. Alveolar bone formation at dental implant dehiscence defects following guided bone regeneration and xenogeneic freeze-dried demineralized bone matrix. Clin Oral Implants Res. 1998;9(6):419.

[2] Arx TV, Cochran DL, Schenk RK, Buser D. Evaluation of a prototype trilayer membrane (PTLM) for lateral ridge augmentation: an experimental study in the canine mandible. Int J Oral Maxillofac Surg. 2002;31(2):190.

[3] Vignoletti F, Matesanz P, Rodrigo D, Figuero E, Martin C, Sanz M. Surgical protocols for ridge preservation after tooth extraction. A systematic review. Clin Oral Implants Res. 2012;23:22.

[4] Rocchietta I, Fontana F, Simion M. Clinical outcomes of vertical bone augmentation to enable dental implant placement: a systematic review. J Clin Periodontol. 2008;35:203.

[5] Aghaloo TL, Moy PK. Which hard tissue augmentation techniques are the most successful in furnishing bony support for implant placement? Int J Oral Maxillofac Implants. 2007;22(7):49.

[6] Wessing B, Lettner S, Zechner W. Guided bone regeneration with collagen membranes and particulate graft materials: a systematic review and meta-analysis. Int J Oral Maxillofac Implants. 2018;33:87.

[7] Rakhmatia YD, Ayukawa Y, Furuhashi A, Koyano K. Current barrier membranes: titanium mesh and other membranes for guided bone regeneration in dental applications. J Prosthodont Res. 2013;57(1):3.

[8] Carpio L, Loza J, Lynch S, Genco R. Guided bone regeneration around endosseous implants with anorganic bovine bone mineral. A randomized controlled trial comparing bioabsorbable versus non-resorbable barriers. J Periodontol. 2000;71(11):1743.

[9] Yoshikawa G, Murashima Y, Wadachi R, Sawada N, Suda H. Guided bone regeneration (GBR) using membranes and calcium sulphate after apicectomy: a comparative histomorphometrical study. Int Endod J. 2002;35(3):255.

[10] Liu J, Kerns DG. Mechanisms of guided bone regeneration: a review. Open Dent J. 2014;8:56.

[11] Mir-Mari J, Benic GI, Valmaseda-Castellon E, Hammerle CHF, Jung RE. Influence of wound closure on the volume stability of particulate and non-particulate GBR materials: an *in vitro* cone-beam computed tomographic examination. Part II. Clin Oral Implants Res. 2017;28(6):631.

[12] Sheikh Z, Qureshi J, Alshahrani AM, Nassar H, Ikeda Y, Glogauer M, Ganss B. Collagen based barrier membranes for periodontal guided bone regeneration applications. Odontology. 2017;105(1):1.

[13] Hurzeler MB, Kohal RJ, Naghshbandi J, Mota LF, Conradt J, Hutmacher D, Caffesse RG. Evaluation of a new bioresorbable barrier to facilitate guided bone regeneration around exposed implant threads—an experimental study in the monkey. Int J Oral Maxillofac Surg. 1998;27(4):315.

[14] Zhao DW, Witte F, Lu FQ, Wang JL, Li JL, Qin L. Current status on clinical applications of magnesium-based orthopaedic implants: a review from clinical translational perspective. Biomaterials. 2017;112:287.

[15] Kim BJ, Piao Y, Wufuer M, Son WC, Choi TH. Biocompatibility and efficiency of biodegradable magnesium-based plates and screws in the facial fracture model of beagles. J Oral Maxillofac Surg. 2018;76(5):1055.

[16] Lin DJ, Hung FY, Yeh ML, Lui TS. Microstructure-modified biodegradable magnesium alloy for promoting cytocompatibility and wound healing *in vitro*. J Mater Sci Mater Med. 2015;26(10):248.

[17] Lavernia EJ, Srivatsan TS. The rapid solidification processing of materials: science, principles, technology, advances, and applications. J Mater Sci. 2010;45(2):287.

[18] Zhang CY, Zeng RC, Liu CL, Gao JC. Comparison of calcium phosphate coatings on Mg–Al and Mg–Ca alloys and their corrosion behavior in Hank's solution. Surf Coat Technol. 2010;204:3636.

[19] Elgali I, Turri A, Xia W, Norlindh B, Johansson A, Dahlin C, Thomsen P, Omar O. Guided bone regeneration using resorbable membrane and different bone substitutes: early histological and molecular events. Acta Biomater. 2016;29:409.

[20] Chen J, Lu S, Tan L, Etim IP, Yang K. Comparative study on effects of different coatings on biodegradable and wear properties of Mg–2Zn–1Gd–0.5Zr alloy. Surf Coat Technol. 2018;352:273.

[21] Chen J, Tan L, Etim IP, Yang K. Comparative study of the effect of Nd and Y content on the mechanical and biodegradable properties of Mg–Zn–Zr–*x*Nd/Y ($x = 0.5, 1, 2$) alloys. Mater Technol. 2018;33(10):659.

[22] Chen J, Tan L, Yu X, Yang K. Effect of minor content of Gd on the mechanical and degradable properties of as-cast Mg–2Zn–*x*Gd–0.5Zr alloys. J Mater Sci Technol. 2018. https://doi.org/10.1016/j.jmst.2018.10.022.

[23] Xu LP, Pan F, Yu GN, Yang L, Zhang EL, Yang K. In vitro and in vivo evaluation of the surface bioactivity of a calcium phosphate coated magnesium alloy. Biomaterials. 2009;30(8):1512.

[24] Tan L, Wang Q, Geng F, Xi XS, Qiu JH, Yang K. Preparation and characterization of Ca–P coating on AZ31 magnesium alloy. Trans Nonferr Met Soc. 2010;20:648.

[25] Delgado-Ruiz RA, Calvo-Guirado JL, Romanos GE. Critical size defects for bone regeneration experiments in rabbit calvariae: systematic review and quality evaluation using ARRIVE guidelines. Clin Oral Implants Res. 2015;26(8):915.

[26] Song GL, Song SZ. A possible biodegradable magnesium implant material. Adv Eng Mater. 2007;9(4):298.

[27] Lin DJ, Hung FY, Lee HP, Yeh ML. Development of a novel degradation-controlled magnesium-based regeneration membrane for future guided bone regeneration (GBR) therapy. Met Basel. 2017;7(11):481.

[28] Klopfleisch R, Jung F. The pathology of the foreign body reaction against biomaterials. J Biomed Mater Res A. 2017;105(3):927.

[29] Franz S, Rammelt S, Scharnweber D, Simon JC. Immune responses to implants—a review of the implications for the design of immunomodulatory biomaterials. Biomaterials. 2011;32(28):6692.

[30] Hao YL, Li SJ, Yang R. Biomedical titanium alloys and their additive manufacturing. Rare Met. 2016;35(9):661.